

Synthesis, Characterization, and Physical Properties of Iron Chalcogenides Fe_xSe , Fe_xTe and $\text{Fe}_x(\text{Se},\text{Te})$

Sahana Rößler, Cevriye Koz, Ulrich Schwarz, Handady L. Bhat¹, Ulrich Burkhardt, Dona Cherian¹, Suja Elizabeth¹, Sashidharan Harikrishnan¹, Mydeen Kamal, John A. Mydosh², Michael Niklas, Yurii Prots, Marcus Schmidt, Ulrike Schmidt, Walter Schnelle, Frank Steglich, Liu Hao Tjeng, Yuri Grin and Steffen Wirth

The recent discovery of superconductivity in iron pnictides by Kamihara *et al.* [1] led to a surge of interest in this class of materials. Within a few months of this seminal work, superconductivity was discovered in several iron-based intermetallic compounds. These are the first non-copper oxide materials that exhibit superconductivity at relatively high temperatures: the highest critical temperature T_c achieved so far is 55 K [2,3]. Among them, tetragonal Fe_xSe has the nominally simplest crystal structure [4], but to obtain a pure PbO-type tetragonal phase is found to be difficult. This is a crucial issue since the physical properties of Fe_xSe are extremely sensitive to the Fe:Se ratio and the highest $T_c \cong 8.5$ K at ambient pressure was observed when the material's composition is closest to 1:1 [5].

In this context, the role played by an excess of Fe in the ternary iron chalcogenides $\text{Fe}_x(\text{Se},\text{Te})$ deserves intense consideration. A ternary material with $x = 1$ has so far been found impossible to obtain, and elemental iron appears to be always present in the synthesized ternary samples. The excess Fe ions are supposed to randomly occupy interstitial sites in the chalcogenide layer [6] and give rise to a pair-breaking effect in the superconducting state [7]. Recent experimental studies clearly demonstrate suppression of superconductivity [5] and localization effects [8] induced by excess Fe.

Here, we present a thorough investigation on synthesis and homogeneity range of binary phases Fe_xSe and Fe_xTe as well as on the growth of single crystals by chemical vapor transport. To scrutinize the subtle effects of chemical composition on ternary materials $\text{Fe}_x(\text{Se},\text{Te})$, the physical properties of single crystalline samples with different compositions are compared. Therefore, in addition to the binary in-house material, we investigated ternary samples obtained from our external collaborators. These specimens were grown using a horizontal Bridgman setup. The details of this single crystal

growth and the implicated characterization have been described elsewhere [9]. Our study of the ternary materials $\text{Fe}_{1.09}\text{Te}_{0.5}\text{Se}_{0.5}$ and $\text{Fe}_{1.04}\text{Te}_{0.5}\text{Se}_{0.5}$ is focused on resistivity, magnetization, linear and nonlinear responses of ac susceptibility. The results depict that iron excess causes a broadening of the superconducting transition, a phase separation in the superconducting state, and a localization of the charge carriers in the normal state.

Synthesis of the binary phases Fe_xSe and Fe_xTe

In our investigation, we concentrate on preparing pure phases of tetragonal Fe_xSe and Fe_xTe as well as the characterization of the synthesized material with respect to homogeneity range and composition. In this context, impurities like hexagonal Fe_xSe and elemental iron are considered.

Fe_xTe adopts the same crystal structure as tetragonal Fe_xSe but does not show superconductivity down to the lowest investigated temperatures. However, the phase exhibits a first order structural transition accompanied by an antiferromagnetic ordering [6,10]. Fe_xTe samples were prepared by the same procedure as described in detail for tetragonal Fe_xSe (see below). According to an analysis of the lattice parameters (Fig. 1), the homogeneity range of Fe_xTe amounts to $1.060(5) < x < 1.155(5)$, which is roughly in conformity with earlier findings [11,12].

Polycrystalline Fe_xSe was prepared by solid state reaction of Fe pieces (99,995%) with Se shots (99,999%) in molar ratios close to 1:1 (typically Fe_xSe with $x = 0.98-1.02$). Glassy carbon crucibles with lid were filled with Fe/Se mixtures and placed in quartz ampoules which were sealed under vacuum (10^{-5} mbar). The first part of the temperature program for the reaction (step I in Fig. 2) is similar to a procedure described earlier [5]. However, in order to improve homogeneity, the ingot was ground in a second step, cold-pressed and annealed

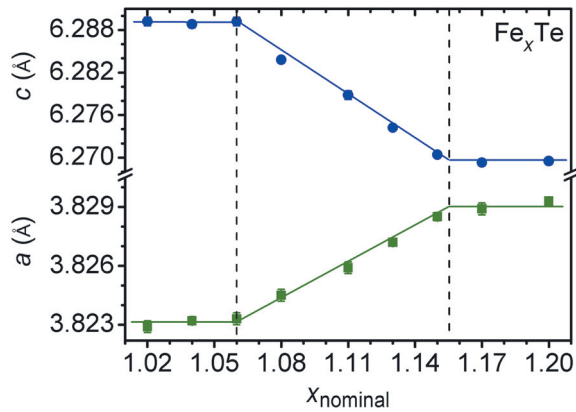


Fig. 1: Lattice parameters at room temperature depending on the nominal composition Fe_xTe . The determinations were performed with LaB_6 as an internal standard in the X-ray powder diffraction experiments. Typical standard deviations amount to $2 \times 10^{-4} \text{ \AA} - 6 \times 10^{-4} \text{ \AA}$ and are, thus, frequently within the size of the symbols.

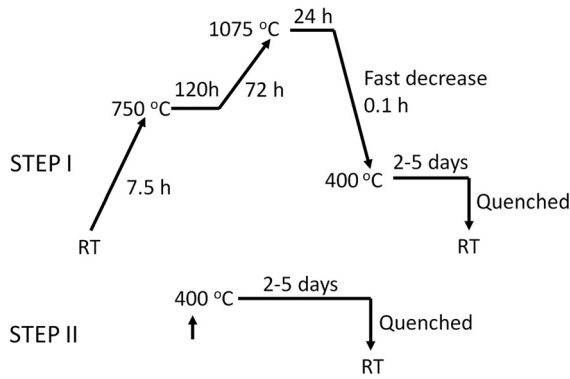


Fig. 2: Temperature program for the synthesis of polycrystalline samples of tetragonal Fe_xSe .

at $400 \text{ }^\circ\text{C}$ for 2–5 days and subsequently quenched in water to room temperature. Except, the reaction process, sample handling and preparation were performed in argon-filled glove boxes.

X-ray powder diffraction experiments exhibit that the prepared polycrystalline Fe_xSe samples mainly contain the tetragonal phase. According to these measurements, a single phase tetragonal Fe_xSe can be synthesized at a molar ratio of 1:1 within experimental error. Even small changes of the composition result in impurity phases. As shown in Figure 3, unreacted iron was observed in samples with Fe excess while surplus of Se induces the formation of hexagonal Fe_xSe .

Samples with a nominal composition $\text{Fe}_{1.00}\text{Se}$ are single phase according to the findings from EDXS or WDXS measurements and X-ray powder diffraction data. However, magnetization measure-

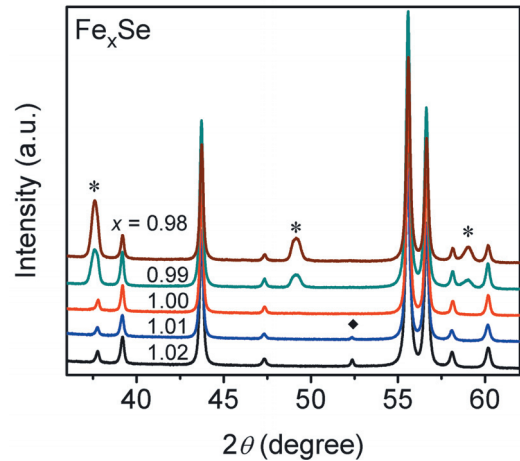


Fig. 3: X-ray diffraction diagram of samples with nominal composition Fe_xSe and tetragonal Fe_xSe as the main phase at room temperature (Impurity phases; hexagonal Fe_xSe marked by * and bcc Fe by ◆)

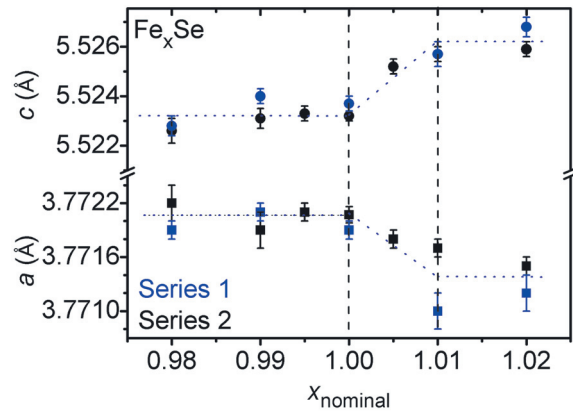


Fig. 4: Lattice parameters of samples with nominal composition Fe_xSe and tetragonal Fe_xSe as the main phase at room temperature. The measurements were performed using TiO_2 as an internal standard in the X-ray powder diffraction experiments.

ments at room temperature indicate that even these samples contain 300 ppm Fe. According to chemical analysis the samples contain less oxygen than the detection limit of 0.05 mass %.

The unit cell dimensions for the investigated compositions Fe_xSe with $0.98 \leq x \leq 1.02$ show very small, but nevertheless systematic changes. The analysis of the lattice parameters narrows the homogeneity range of tetragonal Fe_xSe to $1 \leq x < 1.010(5)$ (Fig. 4).

Single crystals of tetragonal $\text{Fe}_{1.00}\text{Se}$ were grown from polycrystalline material by chemical vapor transport using AlCl_3 as a transporting agent. The evacuated sealed quartz ampoule (diameter 20 mm,

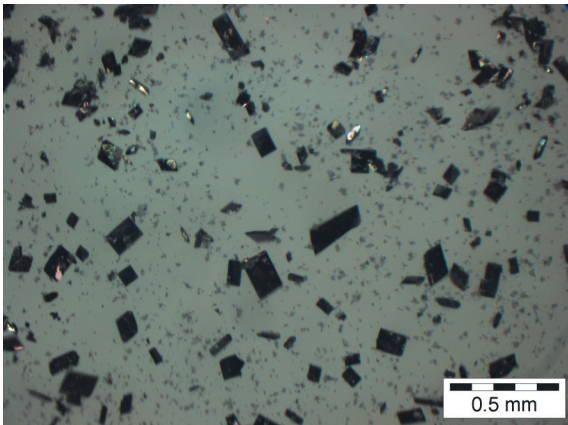


Fig. 5: Fe_xSe single crystals manufactured by chemical vapor transport in a temperature gradient.

length 100 mm) was filled with a mixture of ~ 500 g $\text{Fe}_{1.00}\text{Se}$ powder and ~ 20 mg AlCl_3 and placed inside a horizontal resistance oven. The temperature gradient was $400^\circ\text{C} \rightarrow 300^\circ\text{C}$. The experiments were carried out over two months. Single crystals were washed with ethanol to remove remaining AlCl_3 . As shown in Figure 5, all crystals have the same plate-like morphology.

Regarding to the phase diagram of the system Fe–Se, there are still some uncertainties concerning the homogeneity range of phases and the nature of the phase transitions between tetragonal and hexagonal Fe_xSe . In order to understand the relation between the tetragonal superconducting phase

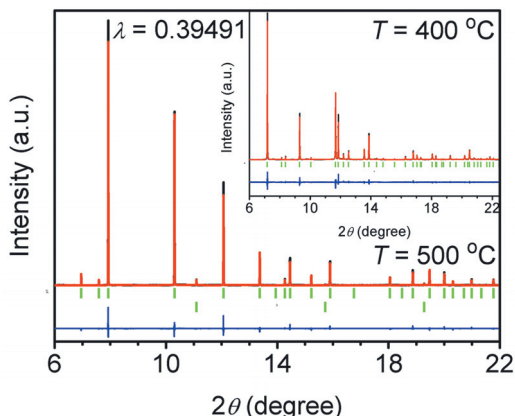


Fig. 6: Synchrotron X-ray powder diffraction data refinement of Fe_xSe at 500°C . Reflection positions of hexagonal Fe_xSe and approximately 3 mol% bcc Fe are represented by the upper and lower green ticks, respectively. The inset shows the XRPD pattern of tetragonal Fe_xSe at 400°C (line positions indicated by green ticks). Red curves show experimental X-ray powder diffraction intensities, the blue lines represent the difference between observed and calculated intensities.

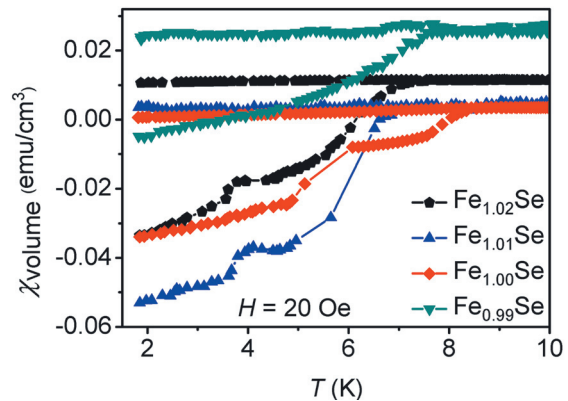


Fig. 7: Magnetic susceptibility of samples with nominal composition Fe_xSe and tetragonal Fe_xSe as the main phase. The discontinuous changes indicate transitions into the superconducting state.

and the hexagonal modification, *in-situ* high-temperature X-ray synchrotron radiation diffraction measurements were performed at the ESRF (Beamline ID31). Tetragonal Fe_xSe (Fig. 6, inset) remains stable with increasing temperatures up to 440°C . Above this temperature, the diffraction data give evidence for a decomposition of tetragonal $\text{Fe}_{1.00}\text{Se}$ into hexagonal Fe_xSe ($x \leq 1$) and traces of bcc Fe in full accordance with earlier reports [13–15]. The transition temperature indicated by the diffraction experiments is in agreement with the findings from DTA measurements.

Figure 7 displays the magnetic susceptibility of Fe_xSe samples at low temperature. The characteristic changes indicate superconducting behavior at low temperatures. The highest $T_c^{\text{onset}} \approx 8.2$ K is observed in samples with a nominal composition $\text{Fe}_{1.00}\text{Se}$ which is in good accordance with previous studies and the findings on the ternary varieties $\text{Fe}_x(\text{Se},\text{Te})$.

Physical properties of ternary phases $\text{Fe}_x(\text{Se},\text{Te})$

The dramatic influence of Fe excess on the electrical transport in ternary phases $\text{Fe}_x(\text{Se},\text{Te})$ is clearly visible in Figure 8, where the resistivity as a function of temperature for the two samples $\text{Fe}_{1.09}\text{Te}_{0.5}\text{Se}_{0.5}$ and $\text{Fe}_{1.04}\text{Te}_{0.5}\text{Se}_{0.5}$ is plotted. Both samples show an onset of the superconducting transitions at around $T_c \sim 15$ K (Fig. 8). Nevertheless, the width of the superconducting transition increases from 1 K to 6 K as the amount of excess Fe increases from 4% to 9%. Further, in

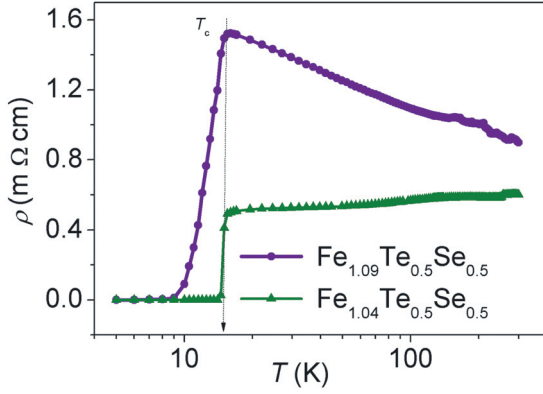


Fig. 8: Resistivity as a function of temperature of samples $\text{Fe}_x(\text{Se},\text{Te})$.

the normal state, for $T < 130$ K, sample $\text{Fe}_{1.04}\text{Te}_{0.5}\text{Se}_{0.5}$ displays metallic behavior ($dp/dT > 0$) whereas a log $1/T$ divergence was observed for $\text{Fe}_{1.09}\text{Te}_{0.5}\text{Se}_{0.5}$. We note that a similar log $1/T$ divergence was also observed in the case of the cuprates [16] and 1111 Fe arsenides [17]. In these cases, this behavior is ascribed to the onset of insulating behavior via disorder-driven electron localization when the superconductivity is suppressed by an external magnetic field. In the present case, however, the log $1/T$ dependence found in the absence of any magnetic field can be ascribed to a similar effect of disorder-induced localization caused by the excess of iron.

To characterize the superconducting state, we performed dc magnetization, as well as, linear, and non-linear ac susceptibility measurements. In our single crystalline samples, the diamagnetic signal was observed only in the zero field cooled (ZFC) measurement protocol. The volume fraction that is screened by superconducting currents was estimated to be about 45% [9]. In Figures 9(a) – (d), the real and imaginary parts of both the fundamental (χ_1) and third-harmonic (χ_3) susceptibility are presented. In a homogeneously superconducting sample, at the transition, the real part of the linear susceptibility χ'_1 always changes monotonically to the full screening value of $-1/4\pi$ whereas the imaginary part χ''_1 either changes monotonically or displays a peak. Also, the magnitude of the third harmonic $|\chi_3| = (\chi_3'^2 + \chi_3''^2)^{1/2}$ forms a peak at T_c . In our samples, $\chi'_1(T)$ does not show a full diamagnetic screening, as seen in Figure 2(a), and $\chi''_1(T)$ displays a shoulder in Figure 2(b) rather than a peak below T_c . Instead of a single sharp peak, $\chi'_3(T)$ and $\chi''_3(T)$ have double peak structures as can be seen

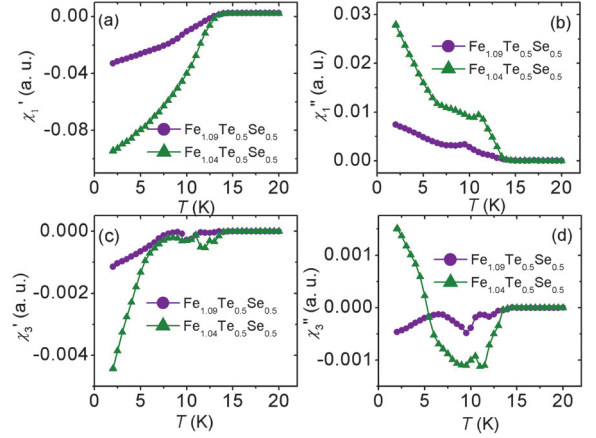


Fig. 9: Ac susceptibility as a function of temperature measured in an ac field of 10 Oe and at a frequency of 1333 Hz for $\text{Fe}_{1.09}\text{Te}_{0.5}\text{Se}_{0.5}$ and $\text{Fe}_{1.04}\text{Te}_{0.5}\text{Se}_{0.5}$ samples. (a) Real part $\chi'_1(T)$, and (b) imaginary part $\chi''_1(T)$ of the linear susceptibility. (c) Real part $\chi'_3(T)$, and (d) imaginary part $\chi''_3(T)$ of the nonlinear susceptibility.

in Figures. 9(c) and (d), respectively. These are clear indications of a phase separation in the superconducting state originating from the magnetic secondary phases.

In an attempt to extract the effective paramagnetic moments, the dc susceptibility obtained from the field cooled (FC) measurement protocol is fitted to $\chi = \chi_0 + C(T - \theta)^{-1}$ in the temperature range 180 K – 300 K. Here, χ_0 is the temperature-independent susceptibility arising from diamagnetic core and, paramagnetic van Vleck contributions, as well as diamagnetic Landau orbital and paramagnetic Pauli spin susceptibilities from conduction electrons. C stands for the Curie constant and θ is the Weiss temperature. It is known that in Fe-containing samples, an analysis of magnetization data is often hampered by the contribution of a ferromagnetic impurity [18, 19], and the inverse susceptibility in the paramagnetic regime can thus be field dependent [9]. Therefore, we utilized the Honda-Owen method [20] to eliminate the impurity contribution with the assumption that the magnetization of the ferromagnetic impurity saturates above a field of about 1 T. In this method, the magnetic susceptibility M/H is plotted against $1/H$ for each temperature [9]. A Curie-Weiss law can be fitted to the extrapolated values of the magnetic susceptibilities in the limit $1/H \rightarrow 0$. These values are then used for the Curie-Weiss fit. From the fit, we obtain $\chi_0 = 0.0019$ emu/g Oe, an effective moment $\mu_{\text{eff}} = 1.49 \mu_B/\text{f. u.}$ and $-\theta$

= 50 K for sample $\text{Fe}_{1.09}\text{Te}_{0.5}\text{Se}_{0.5}$. A similar approach for sample $\text{Fe}_{1.04}\text{Te}_{0.5}\text{Se}_{0.5}$ provided $\chi_0 = 0.0017 \text{ emu g}^{-1} \text{ Oe}$, $\mu_{\text{eff}} = 1.49 \mu_{\text{B}}/\text{f. u.}$, but $-\theta = 88 \text{ K}$. A Curie-Weiss behavior in the iron chalcogenides has been reported by other research groups as well [21] and is attributed to Fe excess with localized moments. However, additional investigations are needed to understand the precise role played by the excess iron in the physical properties of the ternary phases.

Conclusions

A thorough investigation of the phase relations and the chemical composition of synthesized Fe_xSe provided the basis for the preparation of pure tetragonal $\text{Fe}_{1.00}\text{Se}(\text{t})$. Moreover, single crystals of several millimeters edge length could be obtained by chemical transport reactions. However, the finding of 300 ppm Fe even in the hitherto purest powder samples of $\text{Fe}_{1.00}\text{Se}$ stresses the importance of a thorough characterization of the samples since iron excess dramatically influences the magnetic and transport properties. When the amount of excess Fe in samples $\text{Fe}_x(\text{Se}_{0.5}\text{Te}_{0.5})$ is increased from 4 to 9%, a $\log(1/T)$ divergence is observed in the temperature dependence of the resistivity. This result suggests a magnetic-impurity and/or disorder-driven electronic localization by the presence of excess Fe. Further, this excess of Fe seems to possess local moments and lead to a phase-separated superconducting state.

¹ Department of Physics, Indian Institute of Science, Bangalore 560012, India

² Kamerlingh Onnes Laboratory, Leiden University, P. O. Box 5904, 2300 RA Leiden, The Netherlands

References

- [1] Y. Kamihara, T. Watanabe, M. Hirano, and H. Hosono, *J. Am. Chem. Soc.* **130** (2008) 3296.
- [2] G. F. Chen *et al.*, *Phys. Rev. Lett.* **100** (2008) 247002.
- [3] Z. A. Ren *et al.*, *Europhys. Lett.* **83** (2008) 17002.
- [4] F. C. Hsu *et al.*, *Proc. Natl. Acad. Sci. U.S.A.* **105** (2008) 14262.
- [5] T. M. McQueen, Q. Huang, V. Ksenofontov, C. Felser, Q. Xu, H. Zandbergen, Y.S. Hor, J. Allred, A.J. Williams, D. Qu, J. Checkelsky, N.P. Ong, and R. J. Cava, *Phys. Rev. B* **79** (2009) 014522.
- [6] W. Bao, Y. Qui, Q. Huang, M. A. Green, P. Zajdel, M. R. Fitzsimmons, M. Zhernenkov, S. Chang, M. Fang, B. Qian, E. K. Vehstedt, J. Yang, H. M. Pham, L. Špinu, and Z. Q. Mao, *Phys. Rev. Lett.* **102** (2009) 247001.
- [7] L. Zhang, D. J. Singh, and H. M. Du, *Phys. Rev. B* **79** (2009) 012506.
- [8] T. Liu *et al.*, *Phys. Rev. B* **80** (2009) 174509.
- [9] S. Rößler, D. Cheriau, S. Harikrishnan, H. L. Bhat, Suja Elizabeth, J. A. Mydosh, L. H. Tjeng, F. Steglich, and S. Wirth, *Phys. Rev. B* **82** (2010) 144523.
- [10] S. Li, C. de la Cruz, Q. Huang, Y. Chen, J. W. Lynn, J. Hu, Y. L. Huang, F. C. Hsu, K. W. Yeh, M. K. Wu, and P. Dai, *Phys. Rev. B* **79** (2009) 054503.
- [11] H. Ipser, K. L. Komarek, and H. Mikler, *Monatsh. Chemie* **105** (1974) 1322.
- [12] S. Chiba, *J. Phys. Soc. Japan* **10** (1955) 837.
- [13] F. Grönvold, *Acta Chem. Scand.* **22** (1968) 1219.
- [14] S. N. Svendsen, *Acta Chem. Scand.* **26** (1972) 3757.
- [15] J.-C. Grivel, A. C. Wulff, Y. Zhao, N. H. Andersen, J. Bednarčík, and M. v Zimmermann, *Supercond. Sci. Technol.* **24** (2011) 015007.
- [16] Y. Ando, G. S. Boebinger, A. Passner, T. Kimura, and K. Kishio, *Phys. Rev. Lett.* **75** (1995) 4662.
- [17] S. Riggs *et al.*, *Phys. Rev. B* **79** (2009) 212510.
- [18] J. C. Johnston, *Adv. Phys.* **59** (2010) 803.
- [19] A. Leithe-Jasper *et al.*, *Phys. Rev. B.* **70** (2004) 214418.
- [20] K. Honda, *Ann. Phys.* **337** (1910) 1027.
- [21] R. Viennois, E. Giannini, D. van der Marel, and R. Cerni, *J. Solid State Chem* **183** (2010) 769.